JOURNAL OF BONE AND MINERAL RESEARCH
Volume 16, Number 5, 2001

Infrared Microscopic Imaging of Bone: Spatial Distribution of CO_3^{2-}

H. OU-YANG,[1] E.P. PASCHALIS,[2] W.E. MAYO,[3] A.L. BOSKEY,[2] and R. MENDELSOHN[1]

ABSTRACT

This article describes a novel technology for quantitative determination of the spatial distribution of CO_3^{2-} substitution in bone mineral using infrared (IR) imaging at ~6 μm spatial resolution. This novel technology consists of an IR array detector of 64 × 64 elements mapped to a 400 μm × 400 μm spot at the focal plane of an IR microscope. During each scan, a complete IR spectrum is acquired from each element in the array. The variation of any IR parameter across the array may be mapped. In the current study, a linear relationship was observed between the band area or the peak height ratio of the CO_3^{2-} v_3 contour at 1415 cm^{-1} to the PO_4^{3-} v_1,v_3 contour in a series of synthetic carbonated apatites. The correlation coefficient between the spectroscopically and analytically determined ratios ($R^2 = 0.989$) attests to the practical utility of this IR area ratio for determination of bone CO_3^{2-} levels. The relationship forms the basis for the determination of CO_3^{2-} in tissue sections using IR imaging. In four images of trabecular bone the average CO_3^{2-} levels were 5.95 wt% (2298 data points), 6.67% (2040 data points), 6.66% (1176 data points), and 6.73% (2256 data points) with an overall average of 6.38 ± 0.14% (7770 data points). The highest levels of CO_3^{2-} were found at the edge of the trabeculae and immediately adjacent to the Haversian canal. Examination of parameters derived from the phosphate v_1,v_3 contour of the synthetic apatites revealed that the crystallinity/perfection of the hydroxyapatite (HA) crystals was diminished as CO_3^{2-} levels increased. The methodology described will permit evaluation of the spatial distribution of CO_3^{2-} levels in diseased and normal mineralized tissues. (J Bone Miner Res 2001;16:893–900)

Key words: carbonate, bone, infrared imaging, infrared microspectroscopy, Fourier transform infrared

INTRODUCTION

THE MINERAL phase in bone consists of poorly crystalline, carbonate-containing hydroxyapatite (HA). Structurally, replacement of PO_4^{3-} in the HA lattice by CO_3^{2-} leads to a change in lattice dimensions and increased disorder.[1–7] The level of CO_3^{2-} in bone mineral varies with the age of the individual and on average probably exists at ~6 wt%[8] although a range of values has been suggested.[9,10] The level may depend on anatomical location (e.g., trabecular vs. cortical).[11] Levels different from the range encountered in normal bone have been reported for various pathological conditions.[12–16] The relationship between CO_3^{2-} content and the structure of the mineral phase was investigated as a basis for understanding age-related alterations.[17] Carbonate substitution affects the mineral solubility[5,8,9] and the presence of CO_3^{2-} is thought to play a significant role in bone resorption.[18] Studies with point-by-point infrared (IR) microspectroscopy have shown that qualitative changes in the carbonate/phosphate ratio can provide insight into the effects of matrix modification and age in transgenic animals and human bone.[19–21] This work describes the

[1]Department of Chemistry, Rutgers University, Newark, New Jersey, USA.
[2]Mineralized Tissues Laboratory, Hospital for Special Surgery, New York, New York, USA.
[3]Ceramics and Materials Engineering, School of Engineering, Rutgers University, New Brunswick, New Jersey, USA.

development of a method to determine quantitatively the spatial distribution of CO_3^{2-} in mineralized tissues with IR imaging and will enhance our understanding of the significance of carbonate in normal and diseased mineralized tissues.

IR spectroscopic investigations of homogenized bones and teeth[22–24] have shown that CO_3^{2-} ions generally substitute for the two anionic sites in the HA lattice for PO_4^{3-} ions (type B carbonate, the major substitution site in bone and dentin) or for OH^- ions (type A carbonate, which occurs at a significant level in dental enamel). In addition to these insertion sites, a labile carbonate species was identified and is thought to represent surface carbonate.[7] The vibrational mode widely used for identification of these species is the out-of-plane deformation, the v_2 mode, at 879 cm^{-1} in the free ion, which undergoes substitution site-dependent spectral shifts on insertion into the HA lattice. The spatial distribution of the percent of each type of carbonate substitution in bone has been reported elsewhere.[7,8,22–24] Polarized IR studies of the v_2 mode also have provided information about the orientation of the CO_3^{2-} planes in the HA of mineralized turkey tendon.[25]

A limitation of the application of traditional IR spectroscopy to the study of tissues is the necessity for sample homogenization before spectral examination. This process renders it impossible to monitor spatial variations in the tissue constituents. Yet, spatial variations in these properties are evidently a major determinant of biological function. The application of IR microscopy techniques (either using point-by-point methods or array detector-based microscopic imaging) serves to overcome the limitations of sample homogenization. In previous publications[26,27] our laboratories have established the feasibility of acquiring IR microscopic images from normal and abnormal states of mineralized tissue and cartilage. Several IR spectroscopic parameters have been developed for molecular characterization of the mineral and protein components. Although some of these parameters that measure the mineral content, mineral crystallinity, and collagen cross-linking can be applied in both point-by-point Fourier transform infrared (FTIR) microspectroscopy and IR imaging,[28,29] the aforementioned carbonate analysis is not applicable because the v_2 mode of CO_3^{2-} lies outside the operating range of the current generation of mercury-cadmium-telluride array detector elements, which have a low frequency cut-off of $\sim$900 cm^{-1}. The only other CO_3^{2-} mode that is currently feasible for IR imaging is the v_3 mode, which for B type substituted CO_3^{2-}, consists of a spectral doublet with components at $\sim$1419 cm^{-1} and 1450 cm^{-1}. This region of the spectrum overlaps vibrations from both the protein components of the tissue and the embedding material (polymethylmethacrylate [PMMA]) most frequently used for sectioning the tissue, thus rendering quantitative determination of CO_3^{2-} somewhat awkward. Nevertheless, the current study shows the feasibility of using spectral subtraction techniques to overcome spectroscopic interference in this spectral region and therefore to use the v_3 mode for quantitative imaging of CO_3^{2-} in bone.

MATERIALS AND METHODS

Preparation of carbonated HA

Type B carbonate apatites were prepared following the procedure of Penel et al.[30] Briefly, a phosphate solution [0.216 M $(NH_4)_2$ HPO_4 in 30 ml of H_2O and 5 ml of $NH_3 \cdot H_2O$ with varying levels of $NaHCO_3$] was added very slowly over a 3-h period to a constantly stirred calcium-containing solution [0.25 M $Ca(NO_3)_2 \cdot 4H_2O$ dissolved in 30 ml of H_2O and 10 ml of $NH_3 \cdot H_2O$] at 80°C. The precipitates were allowed to mature at 80°C for an additional 2 h. The precipitates were filtered, washed briefly with distilled water, and dried at 60°C overnight. All reagents were analytical grade. Reaction conditions were kept constant except for different levels of sodium bicarbonate.

FTIR and X-ray diffraction analysis

Carbonate apatite crystals were analyzed by FTIR as potassium bromide (KBr) pellets (200:1, wt/wt) on a Mattson RS-1 spectrometer (Mattson, Madison, WI, USA) with 512 scans coadded at 4 cm^{-1} resolution. Interferograms were apodized with a triangular function and Fourier-transformed with one level of zero filling. The sample compartment of the spectrometer was purged constantly with dry air generated from a Whatman gas generator (Whatman, Haverhill, MA, USA).

X-ray spectra were collected on a Siemens D-5000 Powder Diffractometer with automatic sample feeder (Siemens, Iselin, NJ, USA) using Ni-filtered Cu-Kα (1.545 A) radiation. Ground samples were scanned from 24° to 37° (2θ) at 0.05° intervals. Data were accumulated for 4 h to achieve good signal/noise ratios.

Two-dimensional IR analyses

A detailed description of the two-dimensional (2D) IR correlation spectroscopy techniques developed by Noda[31] as applied to the study of HA crystallinity has been published elsewhere.[32] The spectra are normalized to the integrated peak areas to compensate for 2D features arising simply from differences in sample concentrations rather than from alterations in spectral contours.

FTIR imaging

Iliac crest biopsy specimens were acquired as part of routine diagnoses and provided under an Institutional Review Board (IRB)-approved protocol by the Pathology Department of the Hospital for Special Surgery. Samples had been fixed in ethanol, embedded in PMMA, and were cut into $\sim$5-μm-thick sections before placement between two BaF_2 windows on the instrument stage. Spectra were acquired with a BioRad Sting-Ray system (BioRad, Cambridge, MA, USA). In this device, a 64 $\times$ 64 element mercury-cadmium-telluride (MCT) focal plane array detector, mapped to a 400 μm $\times$ 400 μm spot at the focal plane of an IR microscope, is coupled to a step-scan interferometer. Routinely, data from one scan of 1024 steps with 81

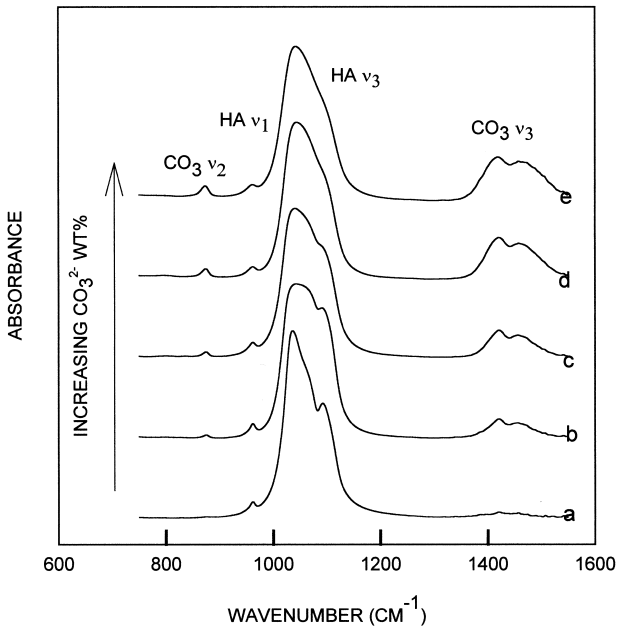

FIG. 1. A series of mid-IR spectra of HA synthesized with (bottom to top) increasing levels of CO_3^{2-} (wt% in the apatitic phase) as follows: a, 1.05; b, 3.33; c, 4.35; d, 7.80, e, 8.78. The spectroscopic features of interest in the current work are labeled.

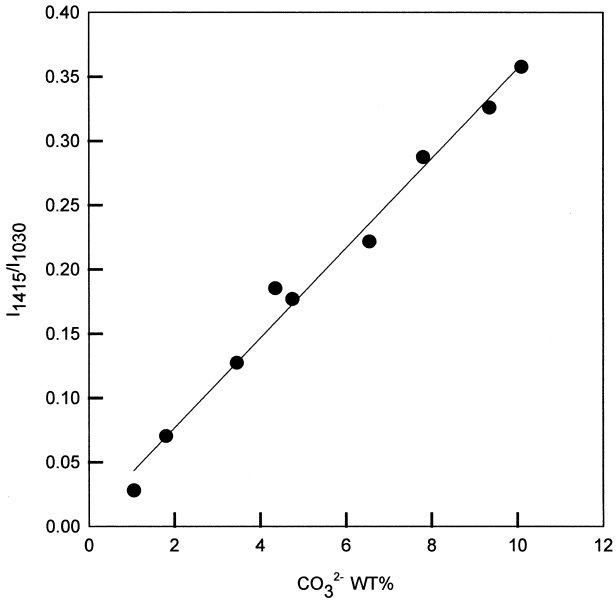

FIG. 2. The linear relationship between the analytically determined weight percent CO_3^{2-} and the intensity ratio of CO_3^{2-} ν_3 mode to the PO_4^{3-} $\nu_{1,}\nu_3$ mode. The regression equation for this determination is $Y = 6.85 \times 10^{-3} + 0.0349X$, where $Y = I_{1415/1030}$ and X = weight percent of carbonate determined analytically. The correlation coefficient is $R^2 = 0.989$.

coadditions at each step were collected at 8 cm^{-1} spectral resolution with one level of zero filling.

Carbonate analysis

The CO_3^{2-} contents of the synthesized apatites were obtained by standard carbon-hydrogen-nitrogen elemental analyses. The content of CO_3^{2-} in the synthetic HA samples was taken as 5× the analytical carbon content.

Data analysis

The coherent crystal lattice dimension in the *c*-axis direction (*c*-axis particle size and perfection) of synthetic apatites was calculated from the Scherrer formula:

$$D = K\lambda/(B^*_{hkl}\cos\theta_{hkl}),$$

where B_{hkl} is the half-width of the *hkl* diffraction peak, λ is the wavelength of the radiation, K is a constant assumed here to be 0.9, and θ_{hkl} is the value in degrees (2θ) of the diffraction maxima for the *hkl* reflection.

IR imaging data were compiled from the 4096 single spectra, which were baseline-corrected in the region of interest before any spectral manipulations. For the quantitative determination of CO_3^{2-}, the contributions of embedding material (PMMA) and organic matrix (collagen) to the original spectra were subtracted based on spectra of the pure compounds. Thus, the intensity of the C = O stretching mode of PMMA at ~1720 cm^{-1} and the amide I frequency at ~1650 cm^{-1} (for collagen) were used as standards for spectral subtraction because there were no mineral contributions at these frequencies in the tissue spectra. For each spectrum in the IR imaging data sets, these correction factors were applied globally to the entire spectrum, thereby minimizing contributions from nonmineral components of the tissue to the CO_3^{2-} ν_3 region.

RESULTS

Determination of CO_3^{2-} in synthetic HA

A series of FTIR spectra (750–1500 cm^{-1}) of synthetic HA with increasing amounts of CO_3^{2-} is shown in Fig. 1. As the levels of CO_3^{2-} increase, several spectral changes are evident. First, the ν_2 band near 875 cm^{-1}, known[18–20] to be comprised of at least three underlying subbands corresponding to A-type CO_3^{2-} at 878 cm^{-1}, B-type CO_3^{2-} at 871 cm^{-1}, and relatively minor nonspecific or surface CO_3^{2-} at 866 cm^{-1} gains in intensity relative to the PO_4^{3-} $\nu_{1,}\nu_3$ contour between 950 and 1200 cm^{-1}. Second, a similar relative intensity increase is observed in the $CO_3^{=}$ ν_3 spectral region. The latter is comprised of a single band near 1419 cm^{-1} in the isolated ion (D_{3h} symmetry), but develops a broad high-frequency shoulder near 1450 cm^{-1} on insertion into the HA lattice. The observed ratio of the 1419–1450 bands is in good accord with the IR data of Rey et al.[7] for B type CO_3^{2-} substitution. This point is discussed in the following paragraph. Finally, increasing levels of CO_3^{2-} are accompanied by broadening of the spectral features within the phosphate $\nu_{1,}\nu_3$ contour, which are indicative of decreased mineral crystallinity/perfection.

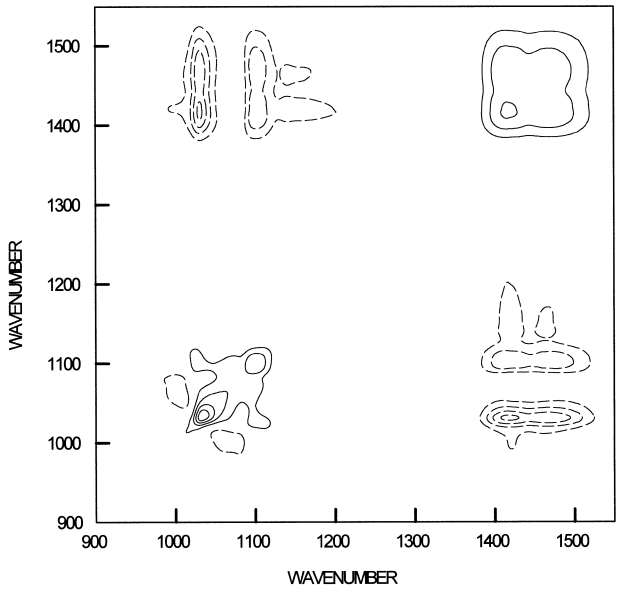

FIG. 3. 2D IR synchronous plot for the series of synthetic samples with increasing levels of CO_3^{2-} ion. The solid lines are positive correlation contours. The dashed lines are negative correlation contours.

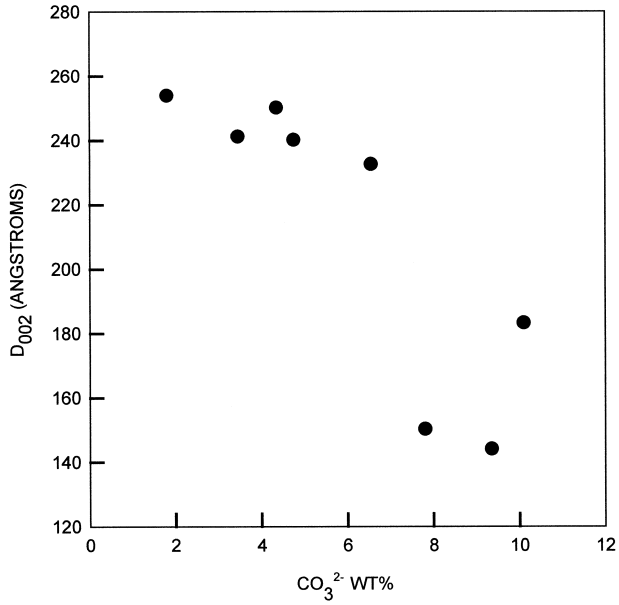

FIG. 5. Calculated *c*-axis particle size/perfection as a function of CO_3^{2-} concentration determined from the Scherrer equation applied to the X-ray powder pattern line widths for the 002 reflection.

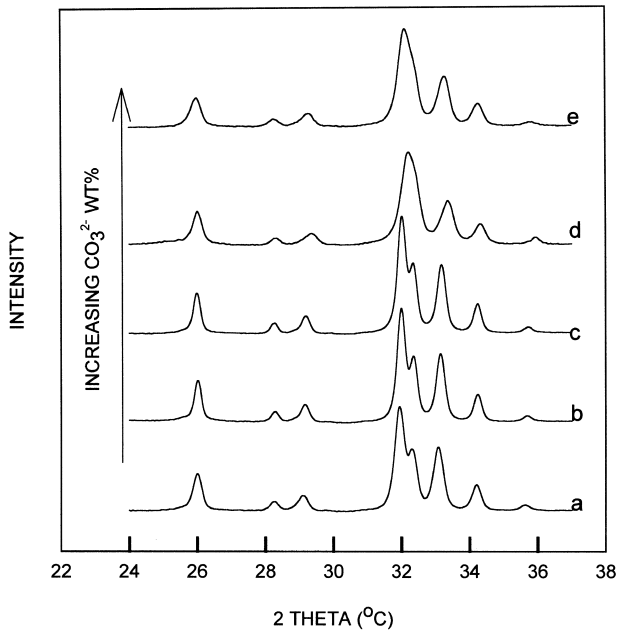

FIG. 4. X-ray powder diffraction patterns for a series of samples of HA synthesized with (bottom to top) increasing levels of CO_3^{2-} (wt% in the apatitic phase) as follows: a, 1.05; b, 3.33; c, 4.35; d, 7.80, e, 8.78.

The quantitative relationship between IR spectral parameters and the analytically determined carbonate levels in these synthetic samples is shown in Fig. 2. The most useful IR parameter for eventual imaging applications is the band area ratio of the CO_3^{2-} v_3 contour to the PO_4^{3-} v_1,v_3 contour. It is noted that comparisons of parameters arising from single bands (peak heights, areas, etc.) are subject to uncertainties arising from thickness variations between samples. Ratios of areas or peak heights therefore are used to control for sample-to-sample variations in the weights of the HA phase used in the analysis. In addition, the use of parameters involving ratios in IR microscopy compensates for sample-to-sample thickness variations in microtomed sections. The drawback of the current measurement is the inherent assumption that the molar integrated area of the phosphate v_1,v_3 contour does not change as the mineral crystallinity/perfection is altered. This conjecture cannot be tested easily so that the aforementioned intensity ratio must be considered as an approximation to the relative carbonate concentration. However, the high value of the correlation coefficient between the spectroscopically and analytically determined ratios in Fig. 2 ($R^2 = 0.989$) attests to the practical utility of the current intensity ratio for IR determination of bone carbonate levels.

Effect of CO_3^{2-} on HA crystallinity/maturity

As is evident from Figs. 1 and 2, increasing levels of carbonate cause substantial alterations in the PO_4^{3-} v_1,v_3 contour. Shape changes in this band are caused by alterations in the positions and widths of the underlying subbands and reflect alterations in mineral crystallinity. Several standard data reduction protocols including curve-fitting, derivative spectroscopy, and Fourier self-deconvolution have been previously used to analyze quantitatively changes in this contour when sample crystallinity/perfection is altered. As discussed elsewhere,[32] each of these methods offers advantages and disadvantages for the analysis of complex contours. Recently, we have shown that the reso-

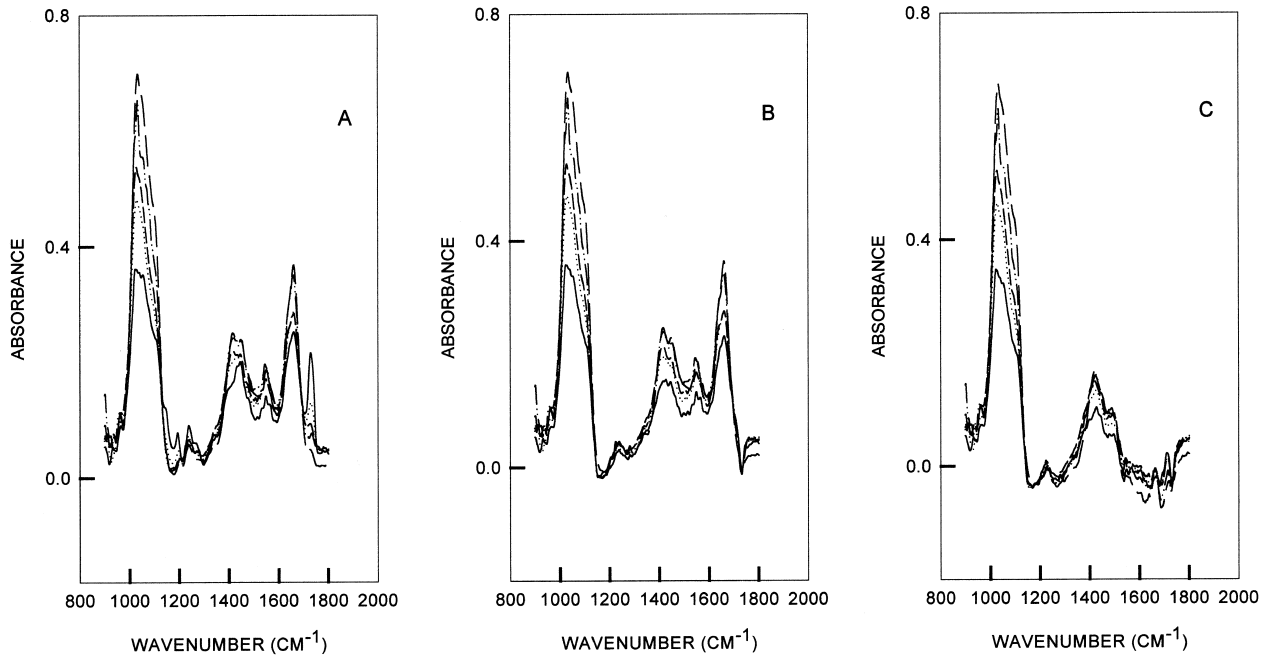

FIG. 6. (A) A series of IR spectra selected from imaging data across trabecular bone showing contributions from PMMA at 1720 cm^{-1} and from the protein amide I mode near 1660 cm^{-1}. (B) The same series of IR spectra as in panel A in which the contributions from PMMA at 1720 cm^{-1} have been removed mathematically while the protein amide I mode near 1660 cm^{-1} are still present. (C) The same series of IR spectra as in panel B from which the protein amide I mode near 1660 cm^{-1} have been removed mathematically.

lution enhancement techniques of 2D IR spectroscopy can be applied to this contour to examine the subtle changes induced by alterations in crystallinity/perfection.[32] Figure 3 shows the 2D synchronous plot generated from the set of samples with increasing levels of CO_3^{2-} in the spectral range of 900-1500 cm^{-1}. The two components of the CO_3^{2-} v_3 contour are correlated negatively with the 1030-cm^{-1} component of the phosphate v_1,v_3 contour. The latter band is known to increase in intensity as mineral crystallinity/perfection is enhanced. In previous studies,[33] we showed that the 1045-cm^{-1} band reflects the amount of B-type CO_3^{2-}. In the current work, a small peak in the 2D synchronous plot is visible at this position, although the bulk of the change in the contour arises from variation of the 1030-cm^{-1} component.

CO_3^{2-}-induced changes in HA crystallinity for this set of synthetic samples also were evaluated with X-ray diffraction. A series of X-ray powder patterns (2θ from 24° to 37°) of HA with increasing levels of CO_3^{2-} is shown in Fig. 4. There is substantial carbonate-induced line broadening in all the reflections, but because of limitations with sample volume, calculations of changes in the *a*-axis dimension were not conclusive. The calculated crystal particle size and perfection derived from the Scherrer equation is plotted for the 002 reflection in Fig. 5 as a function of the level of CO_3^{2-} substitution. Similar trends were noted for the 300 reflection.

Applications to IR microscopy

The primary difficulty with the use of the CO_3^{2-} v_3 mode for IR imaging is the potential interference from overlapped vibrational modes of both the protein component of the tissue and the PMMA embedding material. To compensate for contributions from these constituents to the CO_3^{2-} v_3 mode, a double subtraction protocol was used. The success of this procedure is shown in Fig. 6. The original baseline-corrected spectra from sites across trabecular bone (i.e., varying from low to high levels of mineral) selected from IR imaging data are shown in Fig. 6A. The same set of spectra following the scaled subtraction process to eliminate interference from PMMA is displayed in Fig. 6B. As evident in Fig. 6B, the subtraction process occasionally results in a small residual derivative-like feature, arising from slight spectral shifts in the PMMA C = O stretching band. The contribution of protein to the 1419 cm^{-1} band was estimated from the ratio of the amide I intensity to the 1419 feature in collagen spectra, which was used as a standard for subtraction. The resultant set of spectra is shown in Fig. 6C. The double subtraction process evidently is reasonable, because it results in CO_3^{2-} v_3 contours that closely resemble those in the series of synthetic HA derivatives (compare Fig. 6C with Fig. 1). To illustrate the quantitative determination of relative CO_3^{2-} levels in mineralized tissue as determined from IR microscopic imaging, the results of analyses of four trabecular regions are reported. In addition, a series of 36 spectra were selected from IR imaging data across a region from one of the trabecular bone samples. The spatial variation in the carbonate/phosphate ratio across trabecular bone as monitored by the intensity ratio of the CO_3^{2-} v_3/PO_4^{3-} v_1,v_3 bands following the double subtraction process is shown in Fig. 7A. The highest relative levels of carbonate occur at the edges, with the lowest relative levels

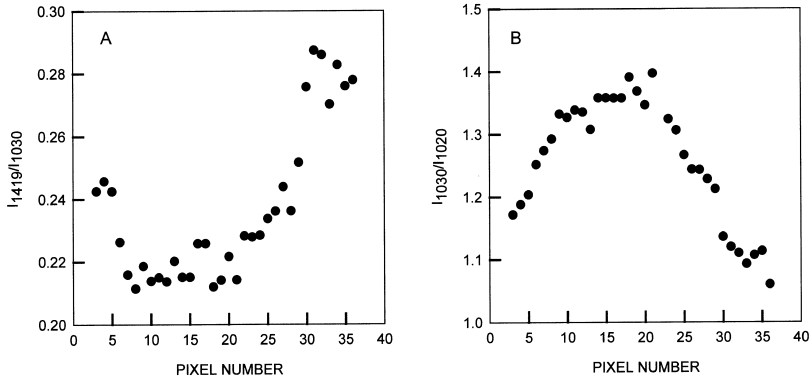

FIG. 7. (A) Variation in the intensity ratio of CO_3^{2-} v_3 mode to the PO_4^{3-} $v_{1,}v_3$ mode across a trabecular bone sample from a human iliac crest biopsy specimen. The spectra from which these data were obtained were selected from the set of IR imaging data shown in Fig. 6. (B) Variation in the intensity ratio of two peaks at 1030 cm^{-1} and 1020 cm^{-1} within the PO_4^{3-} $v_{1,}v_3$ contour across the trabecular bone sample shown in panel A.

evident at the center of the tissue. The variation in mineral crystallinity/perfection as monitored from the intensity ratio (I 1030/I 1020) is plotted in Fig. 7B and shows the trends in the direction opposite to those seen in the carbonate/phosphate levels. The I 1030/I 1020 index is highest at the center of the bone and decreases toward the edges.

Finally, the variation in relative CO_3^{2-} levels in one of 400 μm $\times$ 400 μm sections of trabecular bone as determined from an IR imaging data set is depicted in Fig. 8A. The area ratio of the CO_3^{2-} v_3/PO_4^{3-} $v_{1,}v_3$ bands is converted to weight percent CO_3^{2-} in the mineral phase according the regression equation generated from the data in Fig. 2, color coded, and plotted as an image. In four images of trabecular bone the average CO_3^{2-} levels were 5.95 wt % (2298 data points), 6.67% (2040 data points), 6.66% (1176 data points), and 6.73% (2256 data points). The average value of CO_3^{2-} from these images is $\sim$6.38 $\pm$ 0.14 wt% (7770 data points from the four trabecular bones). In one image of cortical bone from human iliac crest biopsy specimens the CO_3^{2-} levels were 6.40% (3792 data points). The highest levels of CO_3^{2-} were found at the edge of the trabeculae. The highest relative levels of CO_3^{2-}, approaching 10–11%, occur at in a very small number ($<$1%) of pixels near the edges of the bone. Such high levels of carbonate were seen only in this trabecular bone sample. In the other samples studied, the highest weight percent CO_3^{2-} observed was 8% or 9%. A histogram depicting the overall CO_3^{2-} distribution from the four trabecular bone samples are shown in Fig. 8B.

DISCUSSION

The current work describes the first quantitative determination of the spatial variation of CO_3^{2-} in mineralized thin tissue sections using IR imaging. Such a characterization may lead to improved understanding of the functional role of the ion in normal and diseased states. It can be used to correlate variations in microarchitecture with carbonate level or to examine the relative carbonate content adjacent to active osteoclasts or quiescent osteoblasts. It also can be used in tooth sections to distinguish enamel and dentin. The values of the intensity ratio across trabecular bone reveal an average value of 6.38 $\pm$ 0.14 wt% CO_3^{2-} in the apatitic phase. As reported values of bone CO_3^{2-} range from 4 to 7.4%, the average value determined here lies well within the currently accepted range.

The effect of CO_3^{2-} substitution on HA crystallinity as reported previously[5,9,34] also is evident from the 2D IR data shown in Fig. 3. The 2D IR synchronous plots show a strong negative correlation between the 1030-cm^{-1} component of the PO_4^{3-} $v_{1,}v_3$ contour and both components of the CO_3^{2-} v_3 mode. In the current instance the correlation is strengthened by the X-ray diffraction data from the synthetic apatites (Fig. 4). These results are in accord with our previous investigations that show the 1030-cm^{-1} component to be enhanced as the HA crystallinity/perfection is increased. Increased levels of carbonate thus are indicative of an HA phase with reduced crystallinity/perfection.

The determination of CO_3^{2-} in homogenized bone by IR is well documented. Some 35–40 years ago, Emerson and Fischer[35] and Baxter et al.[36] observed a doubling of the v_3 mode. They attributed the additional spectral feature near 1450 cm^{-1} to symmetry lowering of the ion in the tissue. The use of the low-frequency component of v_3 to determine CO_3^{2-} in apatites was shown by Featherstone et al.[37] They determined that the absorbance ratio of this feature to the phosphate v_4 band at 575 cm^{-1} allows an estimate of carbonate levels to better than $\pm$10% in the biologically relevant range of 1–12 wt%. The phosphate v_4 band is precluded from the current study because of detector limitations but the $v_{1,}v_3$ mode used instead offers the advantage of being the strongest band in the IR spectra of mineralized tissues.

An important issue in the current experiments is the substitution pattern of CO_3^{2-}. Rey et al.[7,22,23] have made a thorough study of the effect of the substitution type on the CO_3^{2-} v_3 spectral region. Pure type A CO_3^{2-} in synthetic samples exhibited a well-defined doublet in synthetic samples with components at 1463 cm^{-1} and 1435 cm^{-1}, a pattern not observed in the current bone samples. It is therefore concluded that there is no significant type A substitution in our samples. Type B CO_3^{2-} also presents a well-defined doublet in synthetic samples with components observed by Rey et al.[7] at 1456 and 1422 cm^{-1} with a peak height ratio (calculated from Fig. 3B of Rey et al.[7]) of 1.21. In our synthetic samples, we have observed the same doublet with a linear decrease in the component intensity ratio

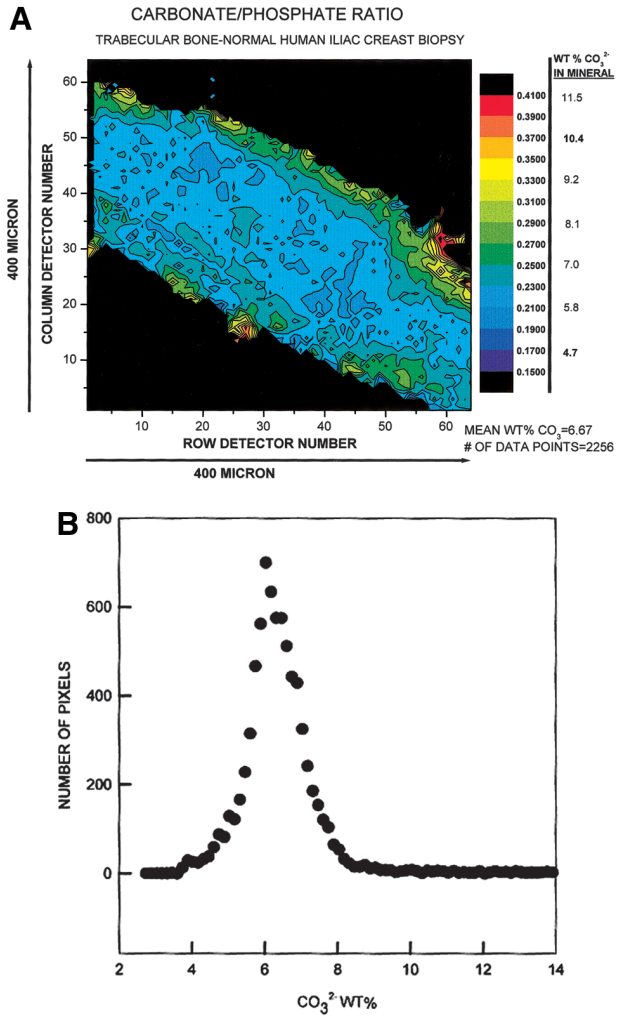

FIG. 8. (A) Variation in the intensity ratio of CO_3^{2-} v_3 mode to the PO_4^{3-} v_1,v_3 mode throughout a trabecular bone sample from a human iliac crest biopsy specimen, acquired from IR microscopic imaging. The color-coding reflects the actual intensity ratios measured from the IR imaging data set. The right hand scale is that derived from the regression equation from the data in Fig. 2. The number of data points used in the analysis is less than 4096 (the number of detectors in the array) because the sample does not fill the field of view. (B) The distribution of CO_3^{2-} values summed over the four trabecular bone samples studied.

from 1.27 to 1.15 as the CO_3^{2-} level increased from 0 to 10%. The variation in the ratio may be related to a differential broadening in the widths of the two components as the CO_3^{2-} level increases. It is evident from a comparison of Rey's data[23] with ours that the current bone samples exhibit negligible interference from type A substitution.

Extensions of the current experiment appear feasible. For example, with appropriate control samples, it should be possible to image spatial variations in both A- and B-type CO_3^{2-} in dental enamel. In addition, the variation of CO_3^{2-} between normal and abnormal states can be determined in a straightforward fashion. In addition, relationships between the spatial distribution of CO_3^{2-} and cellular activity will be accessible.

ACKNOWLEDGMENTS

This work was supported by a Public Health Service Grant (AR 41325) to A.L.B. and R.M. IR images were collected in the IR imaging core at the Hospital for Special Surgery, supported by AR 46121.

REFERENCES

1. Handschin RG, Stern WB 1992 Crystallographic lattice refinement of human bone. Calcif Tissue Int **51:**111–120.
2. Zapanta-LeGeros R 1965 Effect of carbonate on the lattice parameters of apatite. Nature **206:**403–404.
3. Blumenthal NC, Betts F, Posner AS 1975 Effect of carbonate and biological macromolecules on formation and properties of hydroxyapatite. Calcif Tissue Res **18:**81–90.
4. Harries JE, Hukins DW, Hasnain SS 1988 Calcium environment in bone mineral determined by EXAFS spectroscopy. Calcif Tissue Int **43:**250–253.
5. LeGeros RZ, Kijkowska R, Bautista C, LeGeros JP 1995 Synergistic effects of magnesium and carbonate on properties of biological and synthetic apatites. Connect Tissue Res **33:** 203–209.
6. Kim H, Rey C, Glimcher MJ 1996 X-ray diffraction, electron microscopy, and Fourier transform infrared spectroscopy of apatite crystals isolated from chicken and bovine calcified cartilage. Calcif Tissue Int **59:**58–63.
7. Rey C, Collins B, Goehl T, Dickson IR, Glimcher MJ 1989 The carbonate environment in bone mineral: A resolution-enhanced Fourier transform infrared spectroscopy study. Calcif Tissue Int **45:**157–164.
8. Elliott JC 1994 Mineral, synthetic and biological carbonate apatites. In: Structure and Chemistry of the Apatites and Other Calcium Orthophosphates. Elsevier, Amsterdam, The Netherlands, pp. 191–304.
9. LeGeros RZ 1991 Calcium Phosphates in Oral Biology and Medicine. Karger, Basel.
10. Knuuttila M, Lappalainen R, Alakuijala P, Lammi S 1985 Statistical evidence for the relation between citrate and carbonate in human cortical bone. Calcif Tissue Int **37:**363–366.
11. Biltz RM, Pellegrino ED 1981 Skeletal carbonates and acid-base regulation. Miner Electrolyte Metab **5:**1–7.
12. Baig AA, Fox JL, Wang Z, Higuchi WI, Miller SC, Barry, AM Otsuka M 1999 Metastable equilibrium solubility behavior of bone mineral. Calcif Tissue Int **64:**329–339.
13. Driessens FC, van Dijk JW, Borggreven JM 1978 Biological calcium phosphates and their role in the physiology of bone and dental tissues I. Composition and solubility of calcium phosphates. Calcif Tissue Res **26:**127–137.
14. Boskey AL, Gadaleta S, Gundberg C, Doty SB, Ducy P, Karsenty G 1998 Fourier transform infrared microspectroscopic analysis of bones of osteocalcin-deficient mice provides insight into the function of osteocalcin. Bone **23:**187–196.
15. Rey CJ, Lian J, Grynpas M, Shapiro F, Zylberberg L, Glimcher MJ 1989 Non-apatitic environments in bone mineral: FT-IR detection, biological properties and changes in several disease states. Connect Tissue Res **21:**267–273.
16. Gartner J, Simons B 1990 Analysis of calcific deposits in calcifying tendinitis. Clin Orthop **254:**111–120.
17. Legeros R, Balmain N, Bonel G 1987 Age-related changes in mineral of rat and bovine cortical bone. Calcif Tissue Int **41:**137–144.
18. Doi Y, Iwanaga H, Shibutani T, Moriwaki Y, Iwayama Y 1999 Osteoclastic responses to various calcium phosphates in cell cultures. J Biomed Mater Res **47:**424–433.
19. Boskey AL, Gadaleta S, Gundberg C, Doty SB, Ducy P, Karsenty G 1998 FTIR Microspectroscopic analysis of bones

of osteocalcin deficient mice provides insight into the function of osteocalcin. Bone **23:**187–196.
20. Xu T, Fisher L, Bianco P, Longnecker G, Boskey AL, Smith E, Bonadio J, Goldsteins S, Zhao C, Dominguez P, Heegaard AM, Satomura K, Gehron-Robey P, Kulkarni A, Sommer B, Young M 1998 Targeted disruption of the biglycan gene leads to osteoporosis in mice. Nat Genet **20:**78–86.
21. Gadaleta SJ, Boskey AL, Paschalis EP, Carlson C, Menschik F, Baldini T, Peterson M, Rimnac C 2000 A physical, chemical and mechanical study of lumbar vertebrae from normal ovariectomized, and nandrolone decanoate treated cynomolgus monkeys (*Macaca Fascicularis*). Bone **27:**541–550.
22. Rey C, Renugopalakrishnan V, Collins B, Glimcher MJ 1991 Fourier transform infrared spectroscopic study of the carbonate ions in bone mineral during aging. Calcif Tissue Int **49:** 251–258.
23. Rey C, Renugopalakrishnan V, Collins B, Glimcher MJ 1991 A resolution-enhanced Fourier transform infrared spectroscopic study of the environment of the CO_3^{2-} ion in the mineral phase of enamel bone during its formation and maturation. Calcif Tissue Int **49:**259–268.
24. Elliott JC, Holcomb DW, Young RA 1985 Infrared determination of the degree of substitution of hydroxyl by carbonate ions in human dental enamel. Calcif Tissue Int **37:**372–375.
25. Gadaleta SJ, Landis WJ, Boskey AL, Mendelsohn R 1996 Polarized FT-IR microscopy of calcified turkey leg tendon. Connect Tissue Res **34:**203–211.
26. Mendelsohn R, Paschalis EP, Boskey AL 1999 Infrared spectroscopy, microscopy, and microscopic imaging of mineralizing tissues: Spectra-structure correlations from human iliac crest biopsies. J Biomed Optics **4:**14–21.
27. Mendelsohn R, Paschalis EP, Sherman PJ, Boskey AL 2000 IR microscopic imaging of pathological states and fracture healing of bone. Appl Spectrosc **54:**1183–1191.
28. Paschalis EP, DiCarlo E, Betts F, Sherman P, Mendelsohn R, Boskey AL 1996 FTIR microscopic analysis of human osteonal bone. Calcif Tissue Int **59:**480–487.
29. Paschalis EP, Betts F, DiCarlo E, Boskey AL, Mendelsohn R 1997 FTIR Microspectroscopic analysis of normal human cortical and trabecular bone. Calcif Tissue Int **61:**480–486.
30. Penel G, Leroy G, Rey C, Bres E 1998 MicroRaman spectral study of the PO_4 and CO_3 vibrational modes in synthetic and biological apatites. Calcif Tissue Int **63:**475–481.
31. Noda I 1990 Two-dimensional (2D IR) spectroscopy: Theory and applications. Appl Spectrosc **44:**550–561.
32. Gadaleta SJ, Gericke A, Boskey AL, Mendelsohn R 1996 Two-dimensional infrared correlation spectroscopy of synthetic and biological apatites. Biospectroscopy **2:**353–364.
33. Ou-Yang H, Paschalis EP, Boskey AL, Mendelsohn R 2000 Two-Dimensional vibrational correlation spectroscopy of in vitro hydroxyapatite maturation. Biopolymers (Biospectroscopy) **57:**129–139.
34. Termine JD, Posner AS 1966 Amorphous/crystalline interrelationship in bone mineral. Calcif Tissue Res **1:**8–23.
35. Emerson WH, Fischer EE 1962 The infra-red absorption spectra of carbonate in calcified tissues. Arch Oral Biol **7:**671–683.
36. Baxter JD, Biltz RM, Pellegrino ED 1966 The physical state of bone carbonate. A comparative infra-red study in several mineralized tissues. Yale J Biol Med **38:**456–470.
37. Featherstone JDB, Pearson S, LeGeros RZ 1984 An infrared method for quantification of carbonate in carbonated apatites. Caries Res **18:**63–66.

Address reprint requests to:
Dr. Adele L. Boskey
Hospital for Special Surgery
535 East 70th Street
New York, NY 10021, USA

Received in original form July 21, 2000; in revised form November 15, 2000; accepted December 4, 2000.